water

MDPI

Article

Nanoscopic Zero-Valent Iron Supported on MgO for Lead Removal from Waters

Alessio Siciliano * and Carlo Limonti

Department of Environmental and Chemical Engineering, University of Calabria, 87036 Rende (CS), Italy; carlo.limonti@gmail.com

* Correspondence: alessio.siciliano@unical.it

Received: 24 January 2018; Accepted: 25 March 2018; Published: 29 March 2018

Abstract: Lead is one of the most toxic heavy metals that can create a severe risk to water ecosystem health. Zero-valent iron is an effective material for Pb^{2+} removal treatments. In particular, nanoscopic zero-valent iron (nZVI) particles are characterized by high reaction rates; nevertheless, their utilization in water and groundwater remediation techniques requires further investigations. Indeed, it is necessary to define effective methods able to avoid the drawbacks due to the aggregation tendency of nanoparticles and their potential uncontrolled transport in groundwater. In this work, nZVI was supported on magnesium oxide grains (MgO_nZVI) to synthesize an alternative material for lead removal from aqueous solutions. Many experiments were conducted under several operating conditions in order to analyze the effectiveness of the produced material in Pb^{2+} abatement. The performance of MgO_nZVI was also compared with those detected using commercial microscopic Fe^0 (mZVI) as a reactive material. The experimental findings showed a much greater reactivity of the supported nanoscopic iron particles. By means of a kinetic analysis of batch tests results, it was verified that, both for MgO_nZVI and mZVI, the lead abatement follows a pseudo-second-order kinetic law. The reaction rates were affected by the initial pH of the treatment solution and by the ratio between the Fe^0 amount and initial lead concentration. The efficiency of MgO_nZVI in a continuous test was steadily around 97.5% for about 1000 exchanged pore volumes (PV) of reactive material, while by using mZVI, the lead removal was approximately 88% for about 600 PV. X-ray diffraction (XRD) and energy-dispersive spectroscopy EDS analyses suggested the formation of typical iron corrosion products and the presence of metallic lead Pb^0 and Pb^{2+} compounds on exhausted materials.

Keywords: kinetic tests; lead removal; nanoscopic zero-valent iron; water treatment

1. Introduction

The contamination of water bodies and groundwater by toxic heavy metals represents an extremely serious environmental and health issue. Lead is among the metallic pollutants largely widespread in the environment. Indeed, Pb^{2+} ions are commonly found in aquatic systems due to their extensive use in many industrial activities, such as battery manufacturing, mining, refining, painting, metal plating and cleaning, agricultural treatments, and so forth [1,2]. This element is characterized by a high toxicity and can accumulate in human organs, causing severe health harms [3]. Therefore, many efforts are necessary to reduce the level of lead in the water and groundwater. The Pb^{2+} removal treatments from contaminated water and wastewaters include chemical precipitation, ion exchange, membrane filtration, adsorption, electrodialysis, and so forth [3]. Among these different techniques, the use of zero-valent iron (ZVI) has recently gained great attention. Indeed, ZVI-based processes work through many mechanisms including adsorption, reduction, and precipitation/immobilization. For this reason, ZVI is an effective material for the removal of a wide range of both inorganic and organic pollutants (chlorinated organic compounds, metals, and metalloids) [4–7]. In particular, ZVI

is advantageous in the removal of heavy metal ions such as Cr^{6+}, Pb^{2+}, and so forth. In fact, these elements, through the reaction with ZVI, are transformed into less toxic and low-solubility species [4]. The use of metallic iron is particularly suitable in decontamination processes because it is cheap, easy to supply, and harmless. Moreover, ZVI technologies are generally very simple and easy to operate and manage. Specifically, ZVI was widely applied as reactive material in permeable reactive barrier (PRB) technologies [4,6]. Nanoscopic zero-valent iron (nZVI), with respect to microscopic ZVI (mZVI), guarantees a higher reactivity, due to the greater specific surface and more active superficial sites [8–10]. Nevertheless, iron nanoparticles, due to magnetic interactions and high surface energy, tend to aggregate, forming larger agglomerates. This clearly could notably reduce the material reactivity. Furthermore, in groundwater remediation, the residual nanoparticles could be delivered by the flow, causing secondary polluting phenomena [11]. In order to solve these drawbacks, recently, many works have been focused on the development of suitable supports able to fix on their surface the nanoscopic iron particles. Different organic and inorganic supports, such as biochar composites, clay minerals, zeolite, titanium nanotubes, carbon nanotubes, and so forth, have been tested in the removal of many contaminants [2,12–21]. Nevertheless, the development of effective supporting materials still represents a main issue in nZVI technologies [13]. For practical applications in PRB, the reactive materials, besides a high effectiveness, must be economic, easy to prepare, and have a proper granolumetry. Furthermore, the mechanisms and the kinetics of contaminant removal by means of supported nZVI are complex and not well-clarified. Indeed, the process is affected by many parameters, such as the type of support, the amount of supported nZVI, the level of pollutants, the pH, the temperature, the presence of oxidants species, and so forth [8]. Recently, the authors have developed a nZVI-supported material suitable for applications in the decontamination of water and groundwater [22]. Magnesium oxide was exploited as supporting material owing to its ability to create stable interactions with Fe ionic species [23,24]. Moreover, MgO is a common and economic material, and according to the treatment requirements, it can be produced at different particle dimensions to obtain an adequate porosity for in situ processes. Due to these characteristics, it could be suitable in permeable reactive barriers. The reactive material can be easily produced at room conditions by means of a two-phase procedure. In the first step, the MgO grains are impregnated with an iron solution in order to allow the adsorption of Fe^{3+} on the material's surface. In a second phase, the adsorbed Fe^{3+} is reduced to nanoscopic metallic iron by means of the reaction with sodium borohydride $NaBH_4$ [25]. In a previous work, the effectiveness of nanoscale zero-valent iron supported on MgO (MgO_nZVI) in the removal of chromium from natural water was proven. In the present study, the applicability of this material for the abatement of Pb^{2+} from aqueous solutions was investigated. The MgO_nZVI performance was also compared with those detected using microscopic Fe^0 (mZVI) as reactive material. In this regard, many column tests were conducted to evaluate the effects of the reactive material amount (MgO_nZVI or mZVI), initial Pb^{2+} concentration, and pH on the treatment performance. The analysis of batch tests results allowed identification of the reaction kinetics and the process mechanisms. The performance of reactive materials in continuous processes was also tested.

2. Materials and Methods

2.1. Reagents

The experiments were conducted using reagents of analytical grade. Specifically, magnesium oxide (MgO), iron chloride hexahydrate ($FeCl_3 \cdot 6H_2O$), and sodium borohydride ($NaBH_4$) were exploited for the preparation of MgO_nZVI particles; microscopic Fe^0 (200–300 μm) was also tested as reactive material. Lead nitrate ($Pb(NO_3)_2$), HCl (31%), and NaOH (10 N) were used to perform the lead removal tests.

2.2. Synthesis of MgO_nZVI

The synthesis of reactive material was conducted according a two-phase method. In the first step, Fe^{3+} ions were adsorbed on the surface of MgO particles. For this purpose, 16 g of magnesium oxide were added to a solution (0.5 M of Fe^{3+}) obtained through the dissolution of 16.8 g of $FeCl_3 \cdot 6H_2O$ in 90 mL of ethanol and 35 mL of distilled H_2O. This mixture was then mixed at 400 rpm at room conditions for about 24 h. After this period, the solid was filtered and flushed with distilled water. During the second phase, the adsorbed Fe^{3+} ions were reduced to metallic iron through the following reaction with $NaBH_4$ [25]:

$$4Fe^{3+} + 3BH_4{}^- + 9H_2O \rightarrow 4Fe^0 + 3H_2BO_3{}^- + 12H^+ + 6H_2 \uparrow \quad (1)$$

The solid obtained from the first step was added to a solution of sodium borohydride (1 M of B) made by dissolving 4.7 g of $NaBH_4$ into 90 mL of ethanol and 35 mL of distilled H_2O. This mixture was mixed at 200 rpm for about 4 h. After this reaction period, the solid was recovered by filtration and washed with distilled water. The resulting wet MgO_nZVI particles were directly applied in column tests for lead abatement.

2.3. Column Tests

The batch tests were conducted using a small laboratory pilot plant made of a Plexiglas column whose diameter and total height were 2.7 cm and 16 cm, respectively (Figure 1a). The cross section resulted at about 5.72 cm^2. Two proper holes of 0.6 cm were made at the bottom and at a height of approximately 8 cm for the inlet flow and the outflow, respectively (Figure 1a). A permeable membrane was fixed at 2 cm from the base of the column to support the reactive material (Figure 1a).

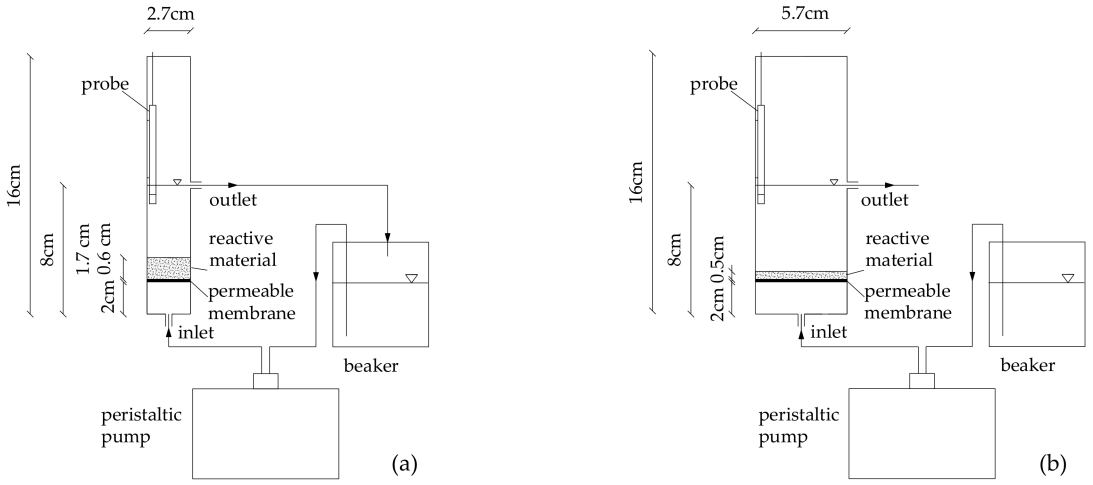

Figure 1. Schemes of the systems used for batch tests (the depth of reactive material in the column was 1.7 cm and 0.6 cm for nanoscopic zero-valent iron supported on magnesium oxide grains (MgO_nZVI) and microscopic zero-valent iron (mZVI), respectively) (**a**) and continuous tests (**b**).

In order to examine performance in lead abatement at typical temperatures of groundwater, the experiments were carried out at a temperature of about 15 ± 1.0 °C. The investigations were aimed at identifying the effects of the initial Pb^{2+} concentration, reactive material quantity, and pH on lead removal. Obviously, the Fe^0 content per unit of mass of MgO_nZVI (Section 3.1) was significantly different compared to commercial mZVI. This made it impossible to conduct the experiments with equal actual Fe^0 amounts of MgO_nZVI and mZVI. Indeed, much more MgO_nZVI would be necessary, and consequently, the equipment and the volumes of treatment solutions could not be the same as used for mZVI. Therefore, the tests were performed keeping constant the overall quantity of

reactive materials. In particular, two set of tests were carried out using 16 g of mZVI or MgO_nZVI. The thickness of material in the column was about of 1.7 cm and 0.6 cm in the tests with MgO_nZVI and mZVI, respectively. This difference was meaningless as the tests were conducted in batch mode. For each set, a total of 15 experiments were carried out by treating standard solutions with initial lead concentration of 5, 10, 30, 50, and 70 mg/L and initial pH of 3, 5, and 7. These pH values were set as the ZVI processes are typically applied under initial conditions that range from strongly acidic to neutral. In each test, the reactive material was put on the permeable membrane and then 300 mL of Pb^{2+} standard solution was recirculated through the cylinder in upflow mode by using a peristaltic pump. The flowrate was set to 52 mL/min in order to obtain a very quick recirculation of standard solution and to therefore ensure the homogeneity of samples withdrawn during the tests for pollutant concentration measurement.

The effectiveness of MgO_nZVI and microscopic iron in the removal of Pb^{2+} was further tested in continuous processes. Because in typical PRB continuous applications the thickness of barrier must be low with respect to the cross section, a larger column was used in these experiments. The system had a diameter of 5.7 cm, a height of 16 cm, and a cross-section area of 25.51 cm^2. The depth of the reactive materials in the column was about 0.5 cm (Figure 1b). Specifically, 23.6 g of MgO_nZVI or 45.8 g of mZVI were used to treat standard solutions characterized by initial concentrations of 50 mg Pb^{2+}/L. The lead solutions were fed through the column in upflow mode with hydraulic flowrates of 5.4 mL/min. The tests were conducted at T = 15 °C ± 1.0 and initial pH = 5.

For each test, the pH was initially set by means of highly concentrated HCl (31%) and NaOH (10N) to limit the solution's dilution, then no further corrections were made. The temperature of the standard lead solution was adjusted to the planned value by use of a heating plate; subsequently, the equipment was placed in a thermostatic refrigerator for the experimental execution. No actions were conducted to remove the dissolved O_2 from the treatment solution.

During the treatments, 5 mL of solutions were periodically withdrawn, filtered at 0.45 µm, and then characterized with regard to the concentration of Pb^{2+}, Fe^{2+}, and Mg^{2+} ions.

2.4. Analytical Methods and Presentation of Results

BET-N_2 adsorption method (BET: Brunauer–Emmett–Teller) was used to measure the specific surface area of MgO_nZVI and mZVI particles. The iron amount adsorbed on magnesium oxide was determined by analyzing the solution detected through the solubilization, at a temperature of 60 °C, of 0.5 g of MgO_nZVI into 50 mL of H_2SO_4 (1:1). X-ray diffraction (XRD), scanning electron microscopy (SEM) and energy-dispersive spectroscopy (EDS) were applied to analyze the reactive materials before and after the reaction with Pb^{2+} solutions.

During the tests, temperature, pH, and O_2 were measured by a multiparametric probe put inside the column (Figure 1); the Pb^{2+}, Fe^{2+}, and Mg^{2+} amount was estimated through the atomic absorption spectrometric methods [26]. Each analysis was conducted in triplicate and the mean value was considered. The relative standard deviation was always less than 5%.

3. Results and Discussion

3.1. Reactive Materials

The magnesium oxide grains exploited in this study had dimensions comprised between 0.6 and 2 mm. As abovementioned, a two-step procedure was adopted to produce MgO_nZVI. After stirring MgO with the $FeCl_3 \cdot 6H_2O$ solution, a red-brownish color appeared, indicating the adsorption of Fe^{3+} onto the surface of the supporting material. At the end of the reaction with $NaBH_4$, the color of the synthesized material turned to black, proving the reduction of adsorbed Fe^{3+} to Fe^0. The XRD analysis of the synthesized particles confirmed the presence of nanoscopic iron included in the grains of MgO (Figure 2). In fact, typical peaks of zero-valent iron were observed. This can be easily noticed by comparing the diffractograms of the synthesized material and commercial microscopic iron (Figure 3).

Clearly, as the MgO is the main constituent of MgO_nZVI, its characteristic peaks were much more marked compared to those of Fe^0 (Figure 2). The EDS analysis further underlined the presence of iron in the synthesized composite (Figure 4). In fact, the main constituents of the material's surface were Fe (50.81%), Mg (29.12%), and O (18.65%). The mass percentages of magnesium and oxygen suggest that these elements were from MgO. Indeed, the low amount of oxygen indicates the absence of Fe oxides and hydroxides and that the iron was in the form of Fe^0, in agreement with the XRD data.

The EDS spectrum of commercial mZVI (Figure 5), obviously, confirmed that the material was almost completely Fe^0 (99.1%). In Figure 6 are shown the SEM images of both materials. Regarding MgO_nZVI, the Fe particles are mainly located in the brighter areas that, as it can be noticed, are well distributed on the grains' surface (Figure 6a).

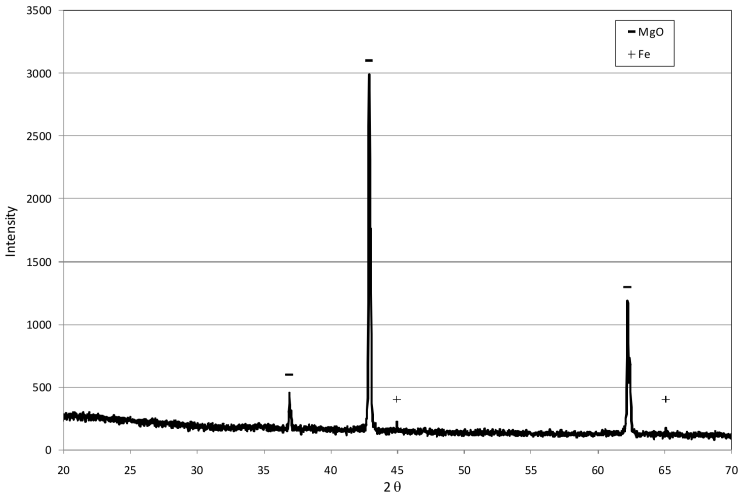

Figure 2. XRD diffractogram of MgO_nZVI particles.

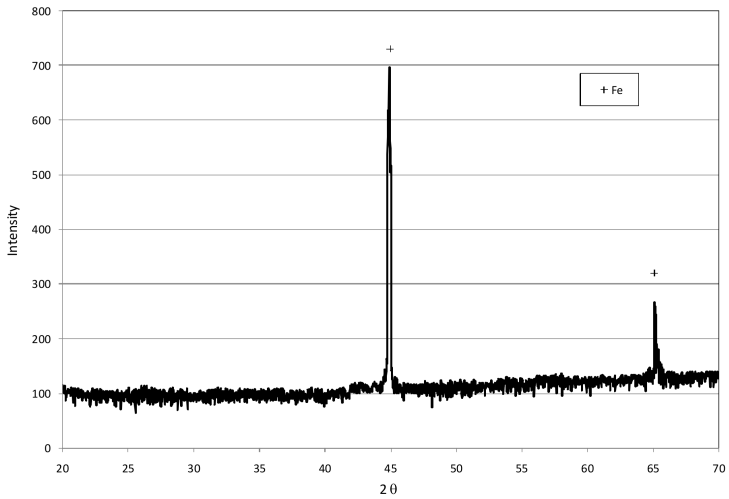

Figure 3. XRD diffractogram of commercial mZVI particles.

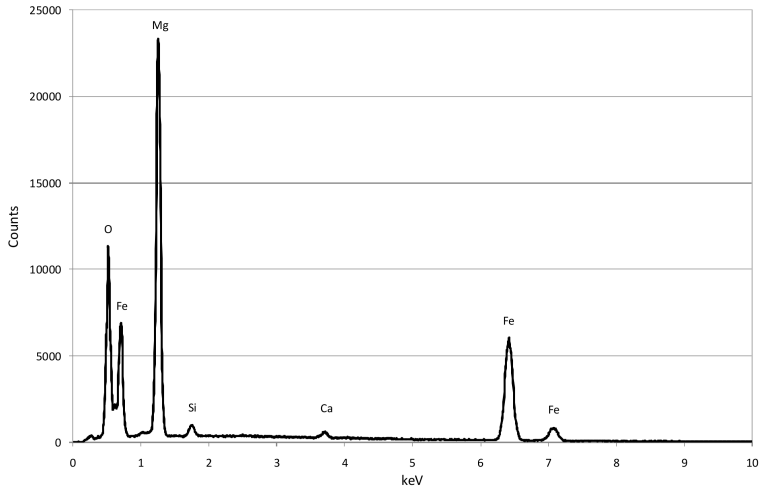

Figure 4. EDS spectrum of MgO_nZVI particles.

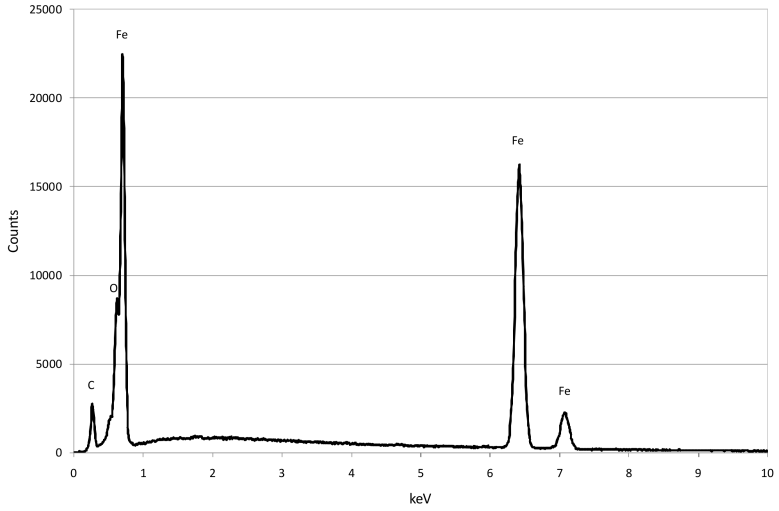

Figure 5. EDS spectrum of commercial mZVI particles.

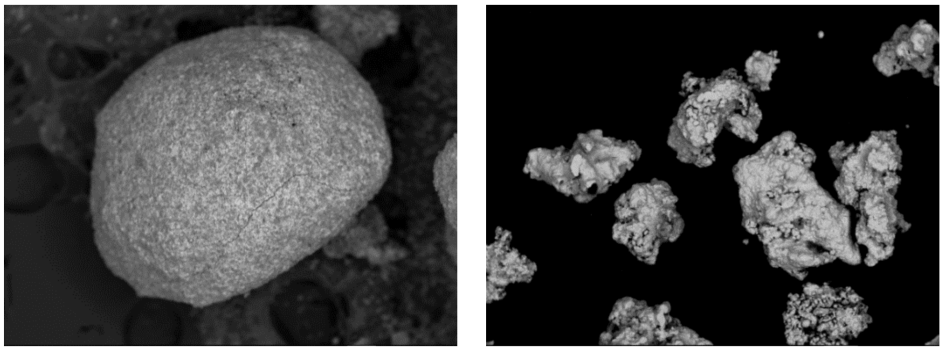

(**a**) (**b**)

Figure 6. Scanning electron microscopy (SEM) images of MgO_nZVI (**a**) and of commercial mZVI particles (**b**).

The actual amount of nanoscopic Fe^0 incorporated into MgO_nZVI, measured as described in the Materials and Methods section, was around 75 mg/g (7.5%). This value is comparable to those detected in other works [27].

The specific surface area of the MgO_nZVI grains was about 24.41 m^2/g, similar to those of other types of reactive materials containing nanoscopic Fe^0 [3,27–29]. The above value was much greater than the specific surface area of mZVI, equal around to 1.1 m^2/g [30].

3.2. Batch Column Tests

3.2.1. Tests with MgO_nZVI

The results of experiments conducted with MgO_nZVI showed the time-decreasing curves typical of batch systems. Satisfactory removals for every operating condition tested were obtained. In particular, at pH = 3, yields of between 82% and 91.1% were achieved in about 30 min (Figure 7a). Even higher abatements during the experiments carried out at initial pH = 5 were reached. Indeed, with this condition, lead removals between 88% and 92.7% were detected after half an hour by treating solutions with initial concentrations up to 30 mgPb/L (Figure 7b). Similar trends to those conducted at pH = 3 were observed with Pb^{2+} amounts of 50 and 70 mgPb/L. However, the performance got worse by increasing the initial pH to 7. In particular, during the experiments with initial lead concentrations higher than 30 mg/L, in comparison with the trends detected at lower pH, a significant reduction of reaction rates was observed (Figure 7c). Nevertheless, in a reaction time of about 1 h, also with the higher initial concentrations, yields greater than 90% were achieved. These results proved the high ability of the reactive material to remove lead ions. Indeed, the achieved performances, taking into account the different operational conditions tested, are comparable with those observed using other types of materials containing nanoscopic zero-valent iron [1,3]. The results detected in this work, being the experiments carried out without the deoxygenation of treatment solutions, proved also that the Pb^{2+} removal can occur efficiently in an aerobic environment [18].

Moreover, it can be observed that the lead abatement decreases in response to the Pb^{2+} concentration of the treatment solution and is affected by the initial pH. Similar statements were reported in other works [1,3]. In particular, Arshadi et al. [3] observed that, using nZVI supported on sineguelas waste, the removal performance decreased when treating solutions with initial concentrations higher than 30 mgPb/L. Other authors stated the negative effect on process efficiency caused by the initial amount of contaminant in the treatment solutions [1]. Furthermore, similar to our results, many previous studies reported the positive influence of initial moderately acidic conditions on Pb removal by means of nZVI [1,3]. However, during our experiments, trends of fast-increasing pH up to alkaline values were always monitored. For example, Figure 8 shows the pH curves detected during the tests conducted with a lead concentration of 30 mgPb/L. The pH enhancements are attributable mainly to the iron corrosion in water. Despite this, the contaminant abatement proceeded past reaching alkaline values (Figures 7 and 8). These outcomes indicate that the lead removal is attributable also to the reaction products. This is clearly a positive aspect, because even with lower reaction rates, the Pb^{2+} removal can evolve at neutral and alkaline pH values.

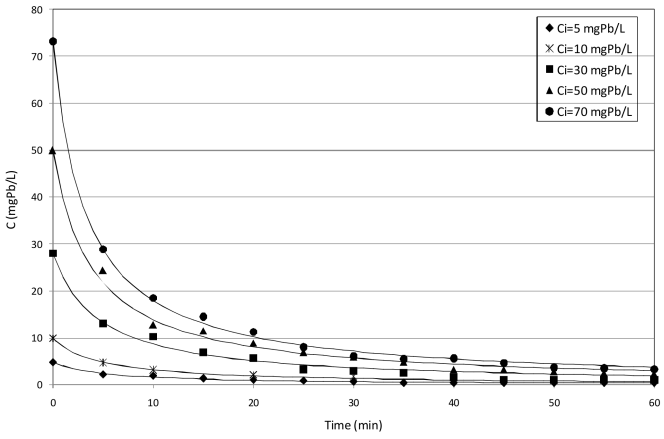

(**a**)

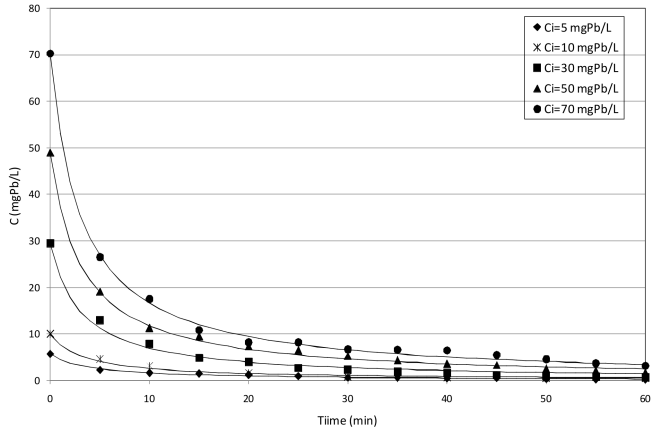

(**b**)

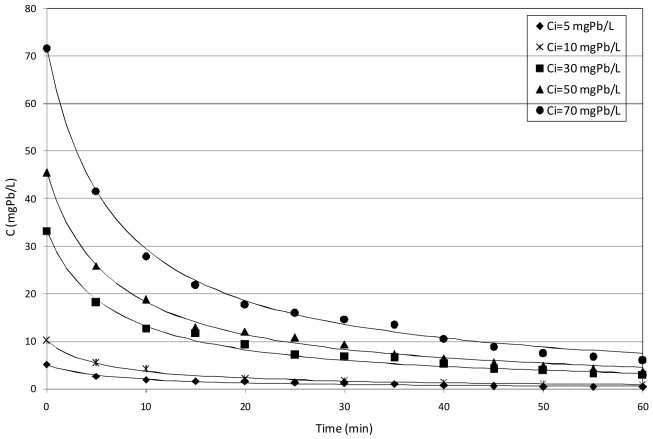

(**c**)

Figure 7. Pb^{2+} concentrations (C) detected during the tests conducted with MgO_nNZVI and different initial lead concentrations (C_i) at initial pH levels of 3 (**a**), 5 (**b**), and 7 (**c**). The continuous trends represent the modeling curves obtained by a second-order kinetic law. The R^2 between the experimental values and the modeling curves were always higher than 0.99.

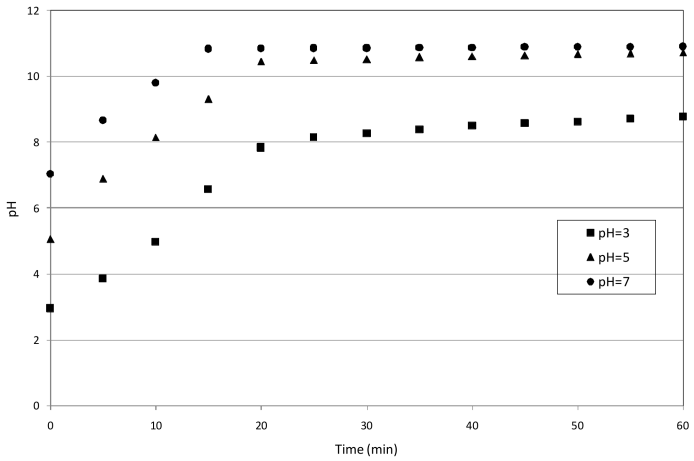

Figure 8. pH trends during the tests conducted with MgO_nZVI and initial Pb^{2+} concentration of 30 mg/L.

Furthermore, the basic pH achieved during the treatment permits limiting the solubilized Fe amount in the treated solutions. In fact, the concentration of Fe ions increased during the initial moments and then rapidly declined as a consequence of pH increase. For every operating condition tested, the amount of solubilized Fe^{2+} was always less than 1.0 mg/L. As an example, in Figure 9 are reported the concentrations of Fe^{2+} monitored in the tests with Pb^{2+} concentration of 30 mgPb/L. The low residual iron is obviously a positive aspect, because the danger of secondary pollution in groundwater is limited. Moreover, only small amounts of Mg^{2+} in the treated solutions were observed. Indeed, maximum amounts of around 3.0 mg/L were observed in the conducted experiments. The low magnesium dissolution is due to the poor solubility of MgO particles. Furthermore, the adsorbed iron nanoparticles reduce the interactions between the MgO grains and the liquid phase. Therefore, the residual concentrations of magnesium ions were always lower than the characteristic values in natural waters.

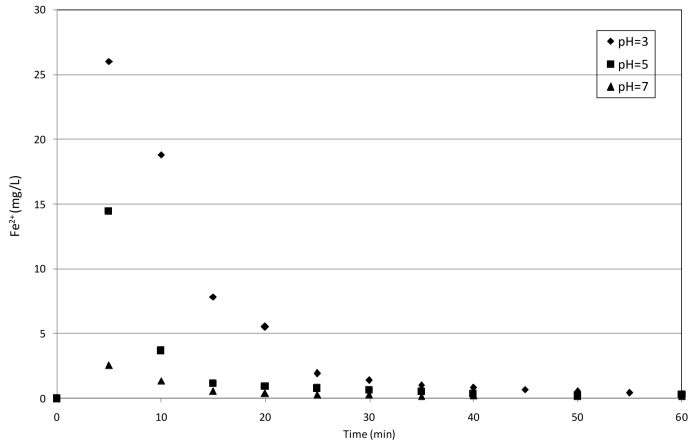

Figure 9. Fe^{2+} concentrations detected during the tests conducted with MgO_nZVI and initial Pb^{2+} concentration of 30 mg/L.

3.2.2. Tests with mZVI

The results of tests conducted with the microscopic iron particles showed lead removal trends (Figure 10) notably slower compared to the curves observed with MgO_nZVI. This caused a reduction of processing yields, particularly when treating solutions with lead concentrations higher than 10 mgPb/L

(Figure 10). Indeed, with these initial pollutant amounts, the abatements were between 78.3% and 74.4% at pH 3, between 87.7% and 75% at pH 5, and between 67.3% and 74.7% at pH 7 (Figure 10), smaller than the values reached with supported nanoparticles. The better performance of MgO_nZVI is even clearer when considering the quantities of Fe^0 in each test. In fact, the actual amount of nanoparticles during the experiments with MgO_nZVI was less than 10% of that of microscopic iron. The above results also demonstrate that the negative effect of initial lead concentration on process performance was more marked when using mZVI. The influence of initial pH was similar to that detected when using nanoscopic iron. In fact, the best performances were obtained at pH = 5, but nevertheless, appreciable abatements were also observed at initial pH=3 and neutral conditions (pH = 7).

Other authors, instead, observed a drastic decline in microscopic iron performance in response to increasing process pH [31]. This discordance with our results is probably imputable to different operating conditions applied for the experimental execution. Moreover, during the tests with mZVI, the pH increases (Figure 11) were always less marked with respect to the trends monitored when using MgO_nZVI. These slower pH increments confirm the weaker activity of microscopic iron particles in lead removal. Moreover, as a consequence of final pH values, notable residual concentrations of dissolved iron in the treated solutions were detected (Figure 12). This, obviously, is a negative aspect of the treatment with mZVI that makes its applicability harder.

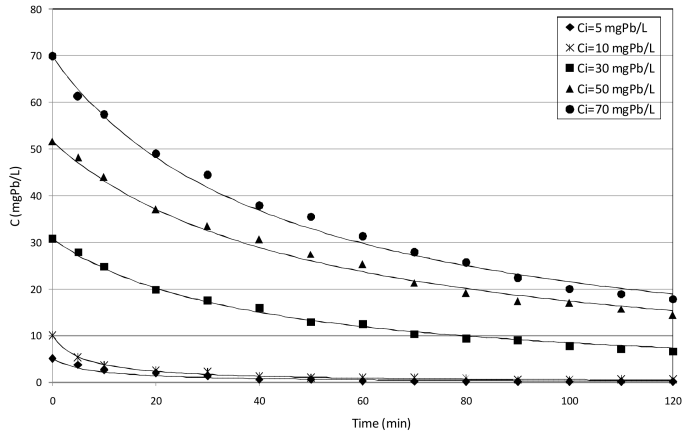

(**a**)

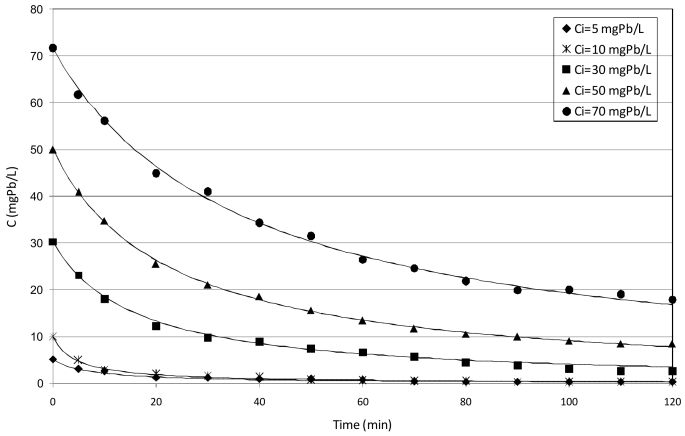

(**b**)

Figure 10. *Cont.*

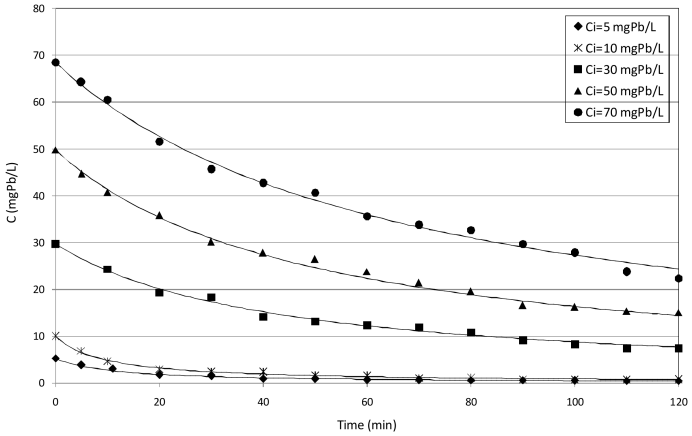

(**c**)

Figure 10. Pb^{2+} concentrations detected (C) during the tests conducted with mZVI and different initial lead concentrations (C_i) at initial pH 3 (**a**), 5 (**b**), and 7 (**c**). The continuous trends represent the modeling curves obtained by a second-order kinetic law. The R^2 between the experimental values and the modeling curves were always higher than 0.99.

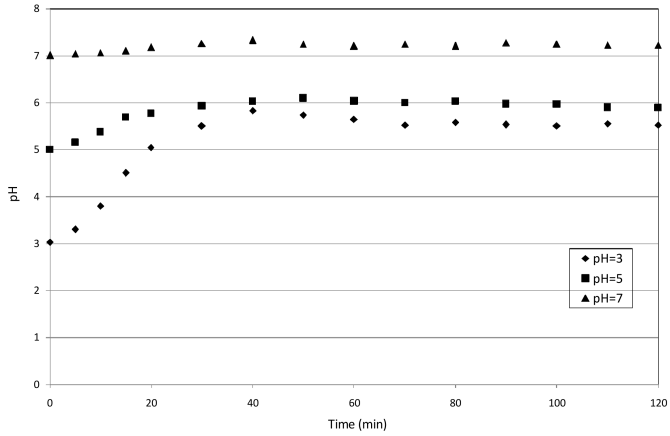

Figure 11. pH trends during the tests conducted with mZVI and initial Pb^{2+} concentration of 30 mg/L.

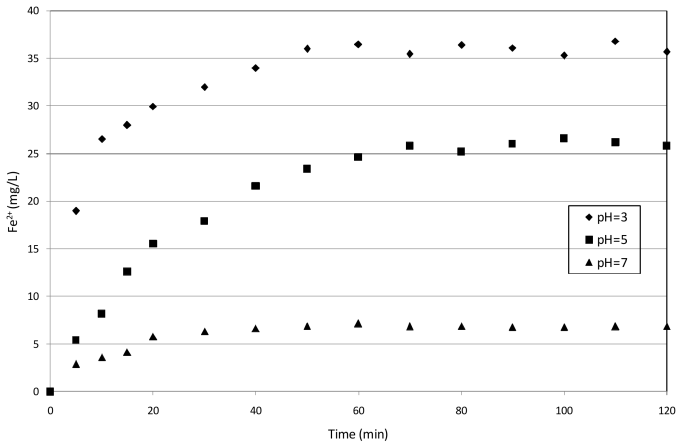

Figure 12. Fe^{2+} concentrations detected during the tests conducted with mZVI and initial Pb^{2+} concentration of 30 mg/L.

3.3. Reaction Mechanisms

The XRD diffractograms of reactive materials after Pb^{2+} removal are shown in Figures 13 and 14. Clearly, their interpretation is made complicated by the presence of different oxides and oxyhydroxides on exhausted materials. Nevertheless, with regard to MgO_nZVI, it can be observed that the peaks of MgO became less marked and those of Fe^0 almost disappeared (Figure 13). On the contrary, some peaks attributable to iron corrosion products, such as γ-FeO(OH), $Fe(OH)_2$, and Fe_2O_3 appeared. Moreover, the XRD analysis indicates the existence of metallic lead Pb^0 and Pb^{2+}, probably in the forms of $Pb(OH)_2$, PbO, and $PbFe_2O_4$ [24] (Figure 13). The diffractogram of mZVI still shows the peaks of Fe^0, suggesting that part of the microscopic particles, probably the inner core, did not react during the treatment (Figure 14). The other peaks indicate the presence of the same compounds identified in the case of the supported composite (Figure 14).

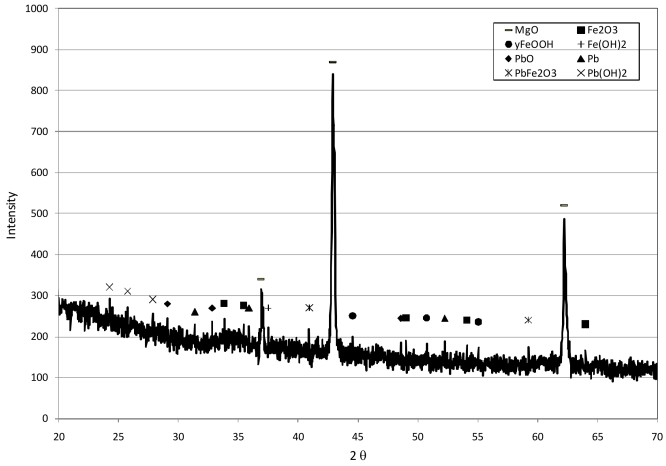

Figure 13. XRD diffractogram of MgO_nZVI after the test conducted with Pb^{2+} concentration of 70 mg/L and initial pH = 5.

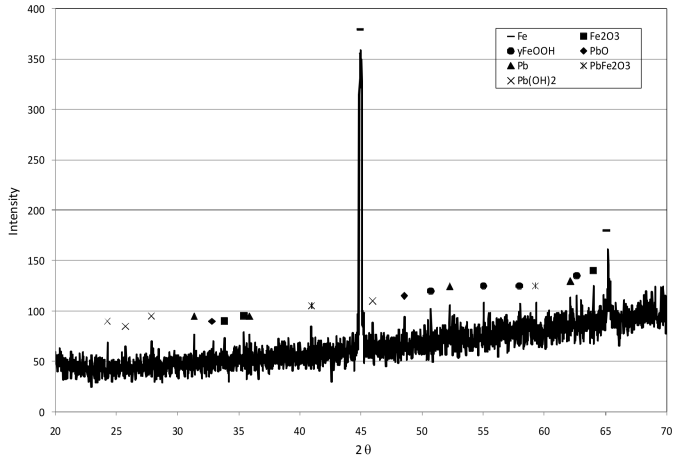

Figure 14. XRD diffractogram of mZVI after the test conducted with Pb^{2+} concentration of 70 mg/L and initial pH = 5.

The EDS analysis of exhausted MgO_nZVI confirmed the presence of lead (16.9%) and suggests the formation of oxides and hydroxides of Fe and Pb (Figure 15). Indeed, compared to the values of fresh MgO_nZVI, the amount of magnesium and iron dropped to 13.4% and 33.8%, respectively, while the quantity of oxygen notably increased up to 34.9%. This, clearly, can be explained by the formation of the reaction products identified by the XRD diffractogram. Also for mZVI the presence of lead was

observed (19.7%) and, in comparison to fresh material, the increase of oxygen amount (18.2%) and the decrease of iron (60.9%) was detected (Figure 16). For both materials, the lead was mainly located in the more luminous zones of the SEM images (Figure 17).

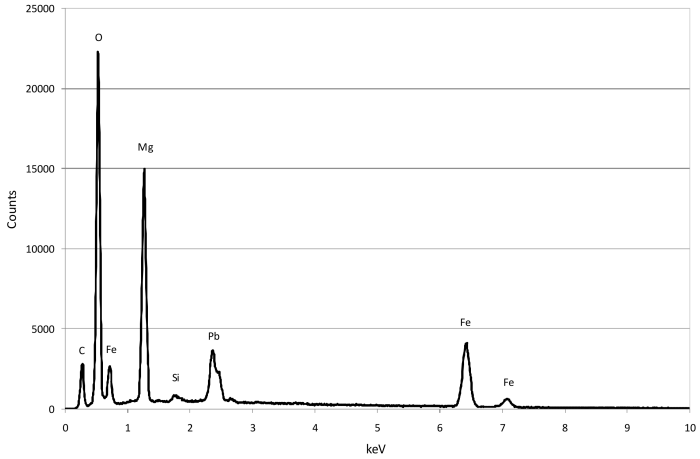

Figure 15. EDS spectrum of MgO_nZVI particles after the lead removal treatment.

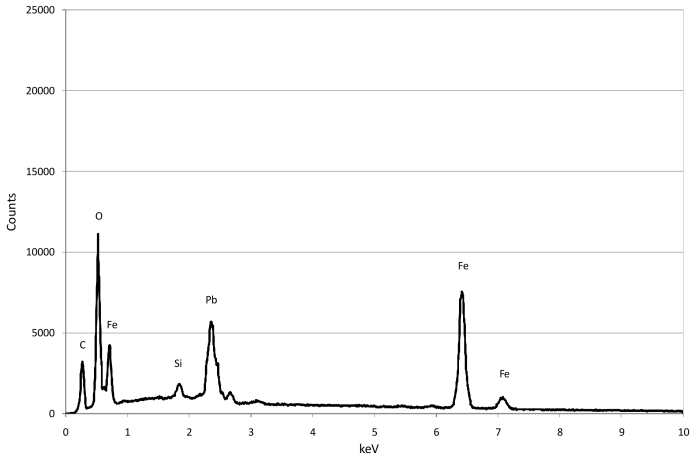

Figure 16. EDS spectrum of commercial mZVI particles after the lead removal treatment.

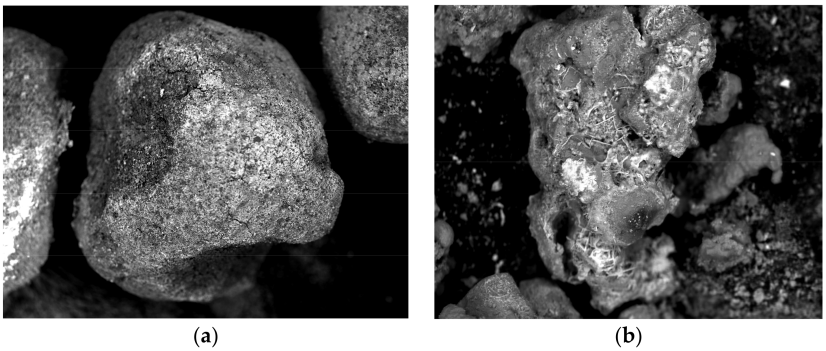

(**a**) (**b**)

Figure 17. SEM images of MgO_nZVI (**a**) and of commercial mZVI particles (**b**) after the lead removal treatment.

The above observations denote that the treatment products resulted from the natural iron corrosion in water, from adsorption mechanisms, and from redox reactions between Fe^0 and Pb^{2+}. Actually, the

removal of lead ions by means of ZVI can evolve according to several reactions that can simultaneously occur. In aqueous solutions, Fe^0 is oxidized by water and oxygen:

$$2Fe^0 + O_2 + 2H_2O \rightarrow 2Fe^{2+} + 4OH^- \quad (2)$$

$$4Fe^{2+} + 4H^+ + O_2 \rightarrow 4Fe^{3+} + 2H_2O \quad (3)$$

The Pb^{2+} ions are adsorbed on the surface of the reactive material and then they are reduced by metallic iron [14,28]:

$$2Fe^0 + 3Pb^{2+} + 4H_2O \rightarrow 3Pb^0 + 2FeOOH + 6H^+ \quad (4)$$

$$2Fe^0 + 3Pb^{2+} + 3H_2O \rightarrow 3Pb^0 + Fe_2O_3 + 6H^+ \quad (5)$$

Under neutral or alkaline conditions, Pb^{2+} and iron species can form insoluble hydroxides:

$$Pb^{2+} + 2OH^- \rightarrow P(OH)_2 \quad (6)$$

$$Fe^{2+} + 2OH^- \rightarrow Fe(OH)_2 \quad (7)$$

$$Fe^{3+} + 3OH^- \rightarrow Fe(OH)_3 \quad (8)$$

Iron hydroxides may be further transformed into metal oxides with release of water [32]:

$$Fe(OH)_3 \rightarrow FeOOH + H_2O \quad (9)$$

By considering our results, in agreement with Pojananukij et al. [29], it is conceivable that iron corrosion products can react with the Pb^{2+} to produce several types of oxide:

$$2FeOOH + Pb^{2+} \rightarrow PbFe_2O_4 + 2H^+ \quad (10)$$

$$FeOOH + Pb^{2+} \rightarrow PbO + Fe^{3+} + OH^- \quad (11)$$

$$Fe_2O_3 + 3Pb^{2+} \rightarrow 3PbO + 2Fe^{3+} \quad (12)$$

The interactions between iron oxyhydroxides and metallic ions have been considered in many other works [7,33–35]. Indeed, Jeen et al. [33] hypothesized the substitution of Fe^{3+} into iron corrosion products and consequently, the formation of insoluble compounds of metallic pollutant. Pratt et al. [34] observed that contaminants can be incorporated in the particulate phase due to the interaction with Fe^{3+} solid species. Manning et al. [35] argued that γ-FeO(OH) acts as a substrate for the production and precipitation of metallic compounds. By considering the above reactions, it can be assumed that the pH increase monitored during the tests is attributable mainly to iron oxidation in water from Fe^0 to Fe^{2+} and Fe^{3+}, as stated also by Kim et al. [13]. Indeed, the H^+ ions released in some reactions [14,28] can be neutralized by the OH^- produced in other ones.

The proposed mechanisms agree with the detected XRD data as well as with the statements of previous studies [2,13,14,29]. Nevertheless, further investigations are necessary to confirm these statements.

3.4. Kinetic Analysis

3.4.1. Tests Conducted with MgO_nZVI

The findings of experiments conducted in the present work proved that many factors affect lead removal by means of MgO_nZVI. In order to better evaluate these influences, a detailed kinetic study was carried out. With this aim, the removal curves obtained during the tests were interpolated using different kinetic equations. The first-order law is commonly applied to model the abatement of several

types of pollutants [7,14,36–38]. In this study, however, the finest fitting between the experimental trends and the simulating curves was achieved with the second-order kinetic [22,36,39]:

$$\frac{dC}{dt} = -k_{obs} \cdot C^2 \quad (13)$$

where C is the Pb^{2+} concentration and k_{obs} is the observed kinetic constant. From this differential equation, the expression of lead concentration as a function of time can be easily obtained:

$$C = \frac{C_i}{k_{obs} \cdot C_i \cdot t + 1} \quad (14)$$

where C_i is the initial Pb^{2+} concentration.

The good matching between the experimental trends and the simulating curves (Figures 7 and 10) proves the appropriateness of the proposed kinetic law.

Through a careful analysis of data obtained by the interpolating of experimental results, a strict relation between the kinetic constants (k_{obs}) and the ratio R_{IL} = Fe/C_i was identified (Figure 18). Specifically, the following function was defined:

$$k_{obs} = k_{max}\left(1 - e^{-\alpha \cdot Fe/C_i}\right) \quad (15)$$

where k_{max} is the maximum kinetic constant and α the rise factor.

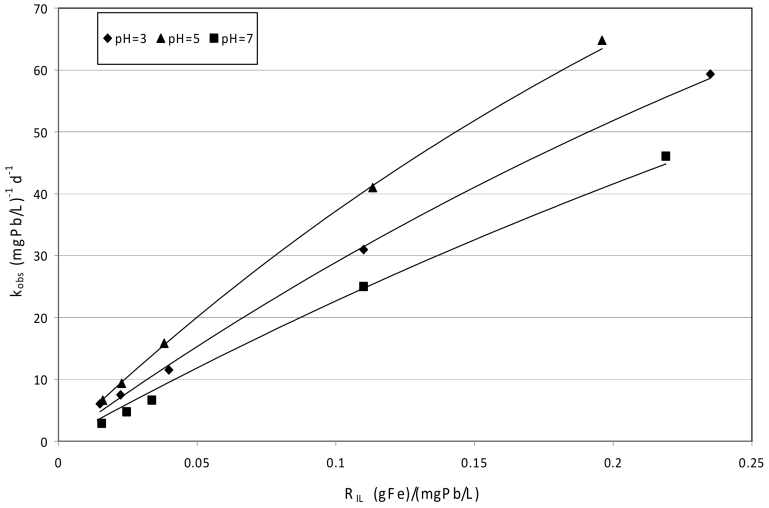

Figure 18. Observed kinetic constant (k_{obs}), detected during the tests with MgO_nZVI, vs. Fe/C_i ratio.

This relation clearly shows that, for a given initial pH, the reaction rate increases with the Fe^0 quantity and declines as consequence of higher initial Pb^{2+} concentration. Indeed, lead ions are oxidants and passivators of metallic iron, therefore, when a greater Pb^{2+} amount is available in the initial solution, more Fe^0 would be quickly oxidized with a consequent activity reduction and a decrease of the kinetic constant. Moreover, for a set reactive material dosage, the increase of the initial pollutant concentration causes an increase in the ratio between initial Pb^{2+} mole numbers and the available active sites of the surface area. Nevertheless, the trends in Figure 18 show a rapid increase of k_{obs} for small values of the Fe/C_i ratio that underlines the high ability of MgO_nZVI to remove lead. In other studies, on the contrary, much slower increases of the kinetic constant were detected [14].

From the curves in Figure 18, the effect of initial pH on lead removal reaction rate can be also noticed. This effect is even more explicit by analyzing the values (Table 1) of rise factor α (Equation (1)) detected by interpolating the curves representative of experiments conducted at different initial pH

values (Figure 18). The results, as above discussed, clearly indicate that the maximum reaction rate is achievable at pH values of around 5. Indeed, this initial pH promotes a more rapid lead abatement during the first minutes of treatment. These findings are in agreement with the statements of other authors [1,3]. In fact, at initial moderately acidic conditions, the electrostatic attraction between the reactive material and lead ions, that increases the adsorption capacity, is favored. Moreover, in this condition, the natural Fe^0 oxidation and passivation in water is less marked. At more highly acidic pH levels, the lead removal decreases because the H^+ competes with Pb^{2+} for adsorption sites [1]. Therefore, due to electrostatic repulsion, the pollutant ions have more difficulty moving toward the MgO_nZVI surface, and consequently, also the reaction between Fe^0 and Pb^{2+} is less effective. A stronger reduction of process performance occurs at higher pH (pH > 5). In these conditions, the increase in the hydroxyl (OH^-) concentration produces the precipitation of lead and iron-insoluble compounds on the MgO_nZVI surface, which negatively affects the material's reactivity. Despite the effects of initial pH values, as already discussed, the lead abatement proceeds, even if less quickly, beyond the corrosion products formation (Figures 7 and 8). Therefore, in agreement with Alowitz et al. [7] and Cheng et al. [40], it can be stated also that iron corrosion products are responsible for a certain abatement of metal pollutants.

Table 1. Kinetic parameters obtained through the interpolation, by means of Equations (15) and (16), of k_{obs} values expressed as function of the Fe/C_i ratio.

	pH	3	5	7
MgO_nZVI	A $(gFe)^{-1}(mgPb/L)$	2.33	3.14	1.81
	α $(molFe)^{-1}(mmolPb/L)$	0.629	0.848	0.489
	k_{max} $(mgPb/L)^{-1}d^{-1}$	139.1	138	136.9
	k_{max} $(mmolPb/m^3)^{-1}d^{-1}$	28.8	28.6	28.4
mZVI	β $(gFe)^{-1}(mgPb/L)$	4.15	4.46	3.54
	β $(molFe)^{-1}(mmolPb/L)$	1.12	1.204	0.956
	k_{max} $(mgPb/L)^{-1}d^{-1}$	36.1	38.5	24.6
	k_{max} $(mmolPb/m^3)^{-1}d^{-1}$	7.5	8	5.1
	k_0 $(mgPb/L)^{-1}d^{-1}$	0.091	0.21	0.15
	k_{max} $(mmolPb/m^3)^{-1}d^{-1}$	0.019	0.043	0.031

3.4.2. Tests Conducted with mZVI

The second-order kinetic law permitted us to accurately model also the results obtained during the tests carried out using mZVI as the reactive material (Figure 10). In this case, the values of k_{obs} obtained through the interpolations showed typical logistic trends which can be expressed by the following function of the Fe/C_i ratio (Figure 19):

$$k_{obs} = \frac{k_{max} \cdot k_0 \cdot e^{\beta \cdot Fe/C_i}}{k_{max} - k_0\left(1 - e^{\beta \cdot Fe/C_i}\right)} \quad (16)$$

where k_{max} and k_0 are, respectively, the maximum and minimum value of the kinetic constant, and β the growth factor. The k_{obs} values increased with exponential trends beyond a threshold value of R_{IL} close to 0.5 gFe/(mgPb/L) [1.85 molFe/(mmolPb/L)] (Figure 19). Below this value, the kinetic constants were quite low for every tested pH level (Figure 19). This suggests that at R_{IL} ratios lower than the critical value, the active surface sites of zero-valent iron are quickly saturated and the pollutant transport to the reactive material becomes rate-limiting [14]. This behavior was not observed in the tests with supported nanoscopic iron, which underlines the higher activity of MgO_nZVI. Indeed, the specific surface, notably greater than that of the microscopic iron used in this study, avoids the saturation of the reactive material for low values of the Fe/C_i ratio. Therefore, with supported nZVI, as previously discussed, the k_{obs} values rapidly grew without an initial lag phase (Figure 18). The greater performance of MgO_nZVI is even clearer when considering that a given value of k_{obs} can be reached

with an actual Fe^0 nanoparticle amount of one order of magnitude lower than the required quantity of microscopic iron (Figures 18 and 19).

The effects of pH on reaction rates were similar to those observed with supported nanoparticles. In fact, the higher k_{obs} were detected at initial moderately acidic conditions (pH = 5), while slower reaction rates at more highly acidic pH values (pH = 3) and at neutral conditions (pH = 7) were monitored.

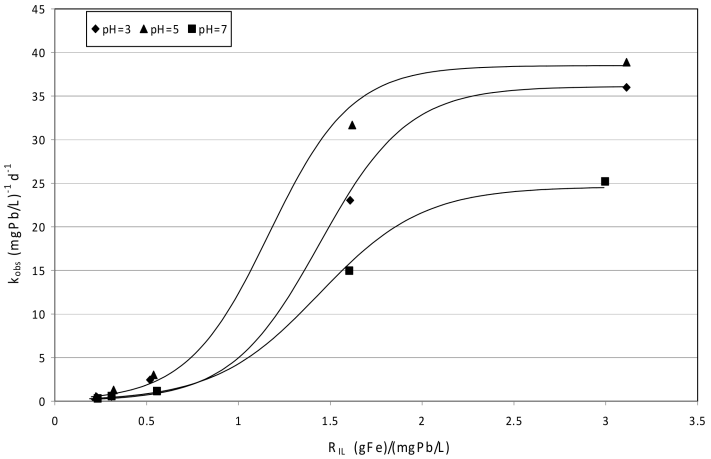

Figure 19. Observed kinetic constant (k_{obs}), detected during the tests with mZVI, vs. Fe/C_i ratio.

3.5. Continuous Tests

The potential application of a reactive material in permeable reactive barriers (PRBs) depends on many factors. Besides the reaction rates, the capacity to treat a high quantity of pollutant and the durability of material are meaningful aspects. In order to evaluate the actual applicability of synthesized MgO_nZVI and commercial mZVI for lead removal in PRBs, two different tests in a continuous mode were carried out.

In the test with MgO_nZVI, the porosity of the reactive material in the column was approximately 0.57 and the hydraulic velocity resulted equal to 6.8 m/d. This high value was set to limit the extent of the experiment. The overall volume of lead solution fed through the system was 16.2 L, which corresponds to about 1865 pore volumes (PV) of reactive material. In Figure 20 is shown the change of normalized Pb^{2+} concentration in the effluent during the overall treatment. Nevertheless the test was conducted with a hydraulic velocity much greater respect the typical values of groundwater [33], a notable performance of the reactive material was detected. Indeed, an average lead removal of about 97.5% was maintained for approximately 1000 exchanged pore volumes (PV). After the breakpoint, a rapid increase of effluent concentration was monitored and the material was completely exhausted at 2200 PV (Figure 20). This value was tenfold higher than that reached in other works, in which zeolite was used as the reactive material and operating conditions comparable to those of the present study were applied [41]. Therefore, the experimental findings prove the high longevity of the synthesized material. Indeed, on the basis of the results of this study, a PRB of 1 m thickness filled with MgO_nZVI, assuming a field flowrate of 0.5 m/d and a concentration of Pb^{2+} in the groundwater of 50 mg/L, could operate for more than five years.

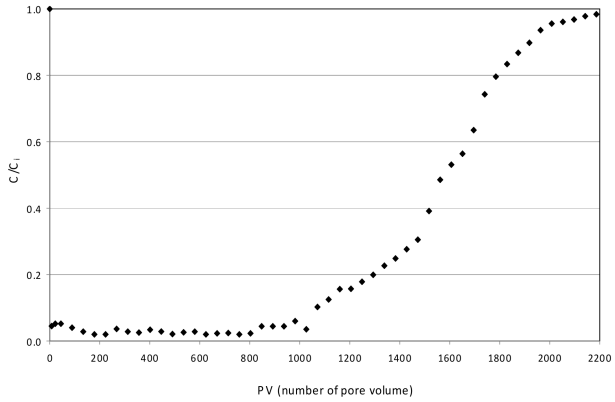

Figure 20. Normalized Pb^{2+} concentration in the effluent (C/C_i) vs. number of exchanged pore volumes (PV) of MgO_nZVI.

The total mass of removed contaminant per amount of the reactive material was about 23.2 $mgPb^{2+}/g$(MgO_nZVI), while, by referring to the actual amount of nZVI included in MgO_nZVI, the removal capacity resulted at 309.55 $mgPb^{2+}/g$(nZVI) [83.6 $mmolPb^{2+}/mol$(nZVI)]. From these values, it is easily understood that the overall performance of MgO_nZVI could be further enhanced by using smaller MgO particles to synthesize the composite. Indeed, the size decrease of the supporting material would allow increasing the quantity of incorporated nZVI, and consequently, to treat even higher amounts of contaminant. Actually, in situ treatments could be exploited MgO_nZVI particles significantly smaller than those used in this work without risks of clogging the reactive material.

During the experiment with mZVI, a volume of Pb^{2+} solution of 7.3 L was fed through the column with a hydraulic velocity of about 6.4 m/d. The porosity of the reactive material in the column was approximately 0.48. The experimental results confirmed the worse efficiency of microscopic iron particles. In fact, in this test, lead abatements of around 88% were reached (Figure 21), about 10% lower with respect to those obtained with MgO_nZVI. The performance remained stable up to a volume of lead solution fed through the column equal to about 600 PV, beyond which the Pb^{2+} in the effluent rapidly increased, and the reactive material was totally exhausted after 1200 PV (Figure 21). The removal ability was 4.80 $mg(Pb^{2+})/g$(mZVI) [1.29 $mmolPb^{2+}/mol$(nZVI)], one magnitude order lower compared to that of nZVI incorporated into MgO_nZVI. The greater amount of removed lead per quantity of ZVI by using supported nZVI, as previously stated, is attributable to its higher specific surface.

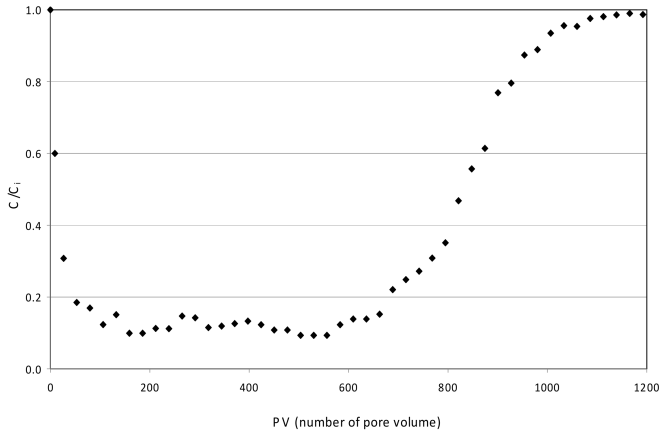

Figure 21. Normalized Pb^{2+} concentration in the effluent (C/C_i) vs. number of exchanged pore volumes (PV) of mZVI.

4. Conclusions

In this paper, the efficiency of lead removal of an alternative reactive material synthesized by supporting iron nanoparticles on MgO grains (MgO_nZVI) was investigated. The characterization of the composite confirmed the presence of iron in the form of Fe^0. The specific surface was about 24.41 m^2/g and the actual amount of Fe^0 resulted at around 75 mgFe/g. The synthesized material showed much better performance than that achieved with commercial microscopic Fe^0 particles, in particular when treating solutions with lead concentrations higher than 10 mgPb/L. Through an analysis of trends detected during many batch column tests, it was identified that a second-order kinetic-type reaction was representative of lead removal using both MgO_nZVI and mZVI. For a given pH, the observed kinetic constants were found to be a function of the Fe/C_i ratio. In particular, by using MgO_nZVI, a rapid increasing of k_{obs} in response to higher Fe/C_i was identified. With mZVI, on the contrary, the relation between k_{obs} and Fe/C_i ratio was a logistic type function characterized by a threshold value below which the kinetic constants increased very slowly. Moreover, by using MgO_nZVI, a given value of k_{obs} can be obtained with an actual Fe^0 nanoparticles quantity of one order of magnitude lower than the required amount of mZVI. For both the reactive materials, the higher reaction rates were obtained at initial moderately acidic conditions (initial pH = 5). Nevertheless, the lead removal evolved also at neutral and basic conditions. The XRD and EDS analyses of exhausted materials allowed identification of the process products. Moreover, the reaction mechanisms have been analyzed and proposed.

The conducted experiments proved also the applicability of MgO_nZVI in continuous treatments. Indeed, abatements of about 97.5% were maintained for about 1000 pore volumes of reactive material, and the overall mass of removed lead was of 309.55 $mg(Pb^{2+})/g(nZVI)$ [83.6 $mmolPb^{2+}/mol(nZVI)$]. These values were notably higher than those monitored with microscopic iron. Therefore, the results of this study support the effectiveness of MgO_nZVI composite as a reactive material for Pb^{2+} removal in PRBs. Nevertheless, further investigations at pilot scale are needed to verify the actual applicability in field conditions.

Acknowledgments: The authors thank Giuseppe Bevilacqua for the technical support.

Author Contributions: Alessio Siciliano planned the work, analyzed the results, and prepared the manuscript. Carlo Limonti performed the experiments.

Conflicts of Interest: The authors declare no conflict of interest.

References

1. Chandraiah, M.R. Facile synthesis of zero valent iron magnetic biochar composites for Pb(II) removal from the aqueous medium. *Alexandria Eng. J.* **2016**, *55*, 619–625.
2. Fu, R.; Yang, Y.; Xu, Z.; Zhang, X.; Guo, X.; Bi, D. The removal of chromium (VI) and lead (II) from groundwater using sepiolite-supported nanoscale zero-valent iron (S-NZVI). *Chemosphere* **2015**, *138*, 726–734. [CrossRef] [PubMed]
3. Arshadi, M.; Soleymanzadeh, M.; Salvacion, J.W.L.; SalimiVahid, F. Nanoscale Zero-Valent Iron (NZVI) supported on sineguelas waste for Pb(II) removal from aqueous solution: Kinetics, thermodynamic and mechanism. *J. Colloid Interface Sci.* **2014**, *426*, 241–251. [CrossRef] [PubMed]
4. Cundy, A.B.; Hopkinson, L.; Whitby, R.L.D. Use of iron-based technologies in contaminated land and groundwater remediation: A review. *Sci. Total Environ.* **2008**, *400*, 42–51. [CrossRef] [PubMed]
5. Li, J.; Li, Y.; Meng, Q. Removal of nitrate by zero-valent iron and pillared bentonite. *J. Hazard. Mater.* **2010**, *174*, 188–193. [CrossRef] [PubMed]
6. Wilkin, R.T.; Su, C.; Ford, R.G.; Paul, C.J. Chromium-Removal Processes during Groundwater Remediation by a Zerovalent Iron Permeable Reactive Barrier. *Environ. Sci. Technol.* **2005**, *39*, 4599–4605. [CrossRef] [PubMed]
7. Alowitz, M.J.; Scherer, M.M. Kinetics of Nitrate, Nitrite, and Cr(VI) Reduction by Iron Metal. *Environ. Sci. Technol.* **2002**, *36*, 299–306. [CrossRef] [PubMed]

8. Li, X.-Q.; Elliott, D.-W.; Zhang, W.-X. Zero-Valent Iron Nanoparticles for Abatement of Environmental Pollutants: Materials and Engineering Aspects. *Crit. Rev. Solid State Mater. Sci.* **2006**, *31*, 111–122. [CrossRef]
9. Liou, Y.H.; Lo, S.-L.; Lin, C.-J.; Kuan, W.H.; Weng, S.C. Chemical reduction of an unbuffered nitrate solution using catalyzed and uncatalyzed nanoscale iron particles. *J. Hazard. Mater.* **2005**, *B127*, 102–110. [CrossRef] [PubMed]
10. Siciliano, A. Use of nanoscale zero-valent iron (NZVI) particles for chemical denitrification under different operating conditions. *Metals* **2015**, *5*, 1507–1519. [CrossRef]
11. Luo, S.; Qin, P.; Shao, J.; Peng, L.; Zeng, Q.; Gu, J.-D. Synthesis of reactive nanoscale zero valent iron using rectorite supports and its application for Orange II removal. *Chem. Eng. J.* **2013**, *223*, 1–7. [CrossRef]
12. Kim, H.; Hong, H.-J.; Jung, J.; Kim, S.-H.; Yang, J.-W. Degradation of trichloroethylene (TCE) by nanoscale zero-valent iron (nZVI) immobilized in alginate bead. *J. Hazard. Mater.* **2010**, *176*, 1038–1043. [CrossRef] [PubMed]
13. Kim, S.A.; Kamala-Kannan, S.; Lee, K.-J.; Park, Y.-J.; Shea, P.J.; Lee, W.-H.; Kim, H.-M.; Oha, B.-T. Removal of Pb(II) from aqueous solution by a zeolite–nanoscale zero-valent iron composite. *Chem. Eng. J.* **2013**, *217*, 54–60. [CrossRef]
14. Ponder, S.M.; Darag, J.G.; Mallouk, T.E. Remediation of Cr(VI) and Pb(II) Aqueous Solutions Using Supported, Nanoscale Zero-valent Iron. *Environ. Sci. Technol.* **2000**, *34*, 2564–2569. [CrossRef]
15. Shu, H.-Y.; Chang, M.-C.; Chen, C.-C.; Chen, P.-E. Using resin supported nano zero-valent iron particles for decoloration of Acid Blue 113 azo dye solution. *J. Hazard. Mater.* **2010**, *184*, 499–505. [CrossRef] [PubMed]
16. Li, Y.; Li, T.; Jin, Z. Stabilization of Fe^0 nanoparticles with silica fume for enhanced transport and remediation of hexavalent chromium in water and soil. *J. Environ. Sci.* **2011**, *23*, 1211–1218. [CrossRef]
17. Fan, M.; Yuan, P.; Zhu, J.; Chen, T.; Yuan, A.; He, H.; Chen, K.; Liu, D. Core–shell structured iron nanoparticles well dispersed on montmorillonite. *J. Magn. Magn. Mater.* **2009**, *321*, 3515–3519. [CrossRef]
18. Zhang, Y.; Li, Y.; Li, J.; Hu, L.; Zheng, X. Enhanced removal of nitrate by a novel composite: Nanoscale zero valent iron supported on pillared clay. *Chem. Eng. J.* **2011**, *171*, 526–531. [CrossRef]
19. Geng, B.; Jin, Z.; Li, T.; Qi, X. Kinetics of hexavalent chromium removal from water by chitosan-Fe^0 nanoparticles. *Chemosphere* **2009**, *75*, 825–830. [CrossRef] [PubMed]
20. Gan, Y.X.; Gan, B.J.; Zhang, L. Electrochemical deposition of iron nanoneedles on titanium oxide nanotubes. *Mater. Lett.* **2011**, *65*, 2992–2994. [CrossRef]
21. Wu, Y.; Yu, H.; Peng, F.; Wang, H. Facile synthesis of porous hollow iron oxide nanoparticles supported on carbon nanotubes. *Mater. Lett.* **2012**, *67*, 245–247. [CrossRef]
22. Siciliano, A. Removal of Cr(VI) from water using a new reactive material: Magnesium Oxide supported nanoscale zero-valent iron. *Materials* **2016**, *9*, 666. [CrossRef] [PubMed]
23. Bond, G.; Molloy, K.C.; Stone, F.S. Reduction of MgO-supported iron oxide: Formation and characterization of Fe/MgO catalysts. *Solid State Ion.* **1997**, *101–103*, 697–705. [CrossRef]
24. Jung, K.-D.; Joo, O.-S.; Kim, C.-S. Study on the structure of Fe/MgO catalysts for H_2S wet oxidation. *Catal. Lett.* **2002**, *84*, 53–57. [CrossRef]
25. Hwang, Y.-H.; Kim, D.-G.; Shin, H.-S. Mechanism study of nitrate reduction by nano zero valent iron. *J. Hazard. Mater.* **2011**, *185*, 1513–1521. [CrossRef] [PubMed]
26. American Public Health Association (APHA). *Standard Methods for the Examination of Water and Wastewater*, 20th ed.; American Public Health Association and Water Environment Federation: Washington, DC, USA, 1998.
27. Liu, T.; Wang, Z.-L.; Yan, X.; Zhang, B. Removal of mercury (II) and chromium (VI) from wastewater using a new and effective composite: Pumice-supported nanoscale zero-valent iron. *Chem. Eng. J.* **2014**, *245*, 34–40. [CrossRef]
28. Zhang, X.; Lin, S.; Lu, X.-Q.; Chen, Z.-L. Removal of Pb(II) from water using synthesized kaolin supported nanoscale zero-valent iron. *Chem. Eng. J.* **2010**, *163*, 243–248. [CrossRef]
29. Pojananukij, N.; Wantala, K.; Neramittagapong, S.; Neramittagapong, A. Equilibrium, kinetics, and mechanism of lead adsorption using zero-valent iron coated on diatomite. *Desal. Water Treat.* **2016**, *57*, 18475–18489. [CrossRef]
30. Zhou, D.; Li, Y.; Zhang, Y.; Zhang, C.; Li, X.; Chen, Z.; Huang, J.; Li, X.; Flores, G.; Kamon, M. Column test-based optimization of the permeable reactive barrier (PRB) technique for remediating groundwater contaminated by landfill leachates. *J. Contam. Hydrol.* **2014**, *168*, 1–16. [CrossRef] [PubMed]

31. Qin, H.; Li, J.; Bao, Q.; Li, L.; Guan, X. Role of dissolved oxygen in metal(loid) removal by zerovalent iron at different pH: Its dependence on the removal mechanisms. *RSC Adv.* **2016**, *6*, 50144. [CrossRef]
32. Gheju, M. Hexavalent chromium reduction with zero-valent iron (ZVI) in aquatic systems. *Water Air Soil Pollut.* **2011**, *222*, 103–108. [CrossRef]
33. Jeen, S.-W.; Blowes, D.W.; Gillham, R.W. Performance evaluation of granular iron for removing hexavalent chromium under different geochemical conditions. *J. Contam. Hydrol.* **2008**, *95*, 76–91. [CrossRef] [PubMed]
34. Pratt, A.R.; Blowes, D.W.; Ptacek, C.J. Products of chromate reduction on proposed subsurface remediation material. *Environ. Sci. Technol.* **1997**, *31*, 2492–2498. [CrossRef]
35. Manning, B.A.; Kiser, J.R.; Kwon, H.; Kanel, S.R. Spectroscopic investigation of Cr(III)- and Cr(VI)-treated nanoscale zerovalent Iron. *Environ. Sci. Technol.* **2007**, *41*, 586–592. [CrossRef] [PubMed]
36. Siciliano, A.; De Rosa, S. Experimental formulation of a kinetic model describing the nitrification process in biological aerated filters filled with plastic elements. *Environ. Technol.* **2015**, *36*, 293–301. [CrossRef] [PubMed]
37. Shi, L.-N.; Lin, Y.-M.; Zhang, X.; Chen, Z.-L. Synthesis, characterization and kinetics of bentonite supported nZVI for the removal of Cr(VI) from aqueous solution. *Chem. Eng. J.* **2011**, *171*, 612–617. [CrossRef]
38. Siciliano, A.; De Rosa, S. An experimental model of COD abatement in MBBR based on biofilm growth dynamic and on substrates' removal kinetics. *Environ. Technol.* **2016**, *37*, 2058–2071. [CrossRef] [PubMed]
39. Siciliano, A.; Stillitano, M.A.; De Rosa, S. Biogas production from wet olive mill wastes pretreated with hydrogen peroxide in alkaline conditions. *Renew. Energy* **2016**, *85*, 903–916. [CrossRef]
40. Cheng, F.; Muftikian, R.; Fernando, Q.; Korte, N. Reduction of nitrate to ammonia by zero-valent iron. *Chemosphere* **1997**, *35*, 2689–2695. [CrossRef]
41. Obiri-Nyarko, F.; Kwiatkowska-Malina, J.; Malina, G.; Kasela, T. Geochemical modelling for predicting the long-term performance of zeolite-PRB to treat lead contaminated groundwater. *J. Contam. Hydrol.* **2015**, *177–178*, 76–84. [CrossRef] [PubMed]